Controllable excitation transfer based on the coupling of an atom with a finite-size Su-Schrieffer-Heeger chain

Da-Wei Wang, Chengsong Zhao, Junya Yang, Ye-Ting Yan, and Ling Zhou
School of Physics, Dalian University of Technology, Dalian 116024, People's Republic of China

(Received 21 November 2023; accepted 8 February 2024; published 11 March 2024)

We propose a scheme to control excitation transfer between an atom and the ends of the Su-Schrieffer-Heeger (SSH) chain. When the finite SSH chain is in the topological phase, and the frequency of the atom is resonant with the center frequency of the SSH chain, an effective transition between the atomic excited state and the band-gap states can be obtained. The system can be equal to the three-states model. Under this case, we can adiabatically transfer the atomic excitation to one of the ends of the SSH chain. Which end of the SSH chain is the receiver depends on which sublattice of the cell the atom is coupled to. Furthermore, the excitation can also be transferred from the atom to the ends of the chain by fixing the parameters under the dynamic evolution. Our paper provides a method for realizing controllable quantum information transfer based on the coupling of an atom with topological matter.

DOI: 10.1103/PhysRevA.109.033708

I. INTRODUCTION

Topological systems have attracted a great deal of interest and attention in quantum physics due to their many interesting properties, including robustness to local decoherence and potential applications in quantum information processes [1–4]. The chiral edge states of topological photonic systems yield directional transport of photons and phonons, which has been exploited in the design of amplifiers and topological lasers [5–8]. The transport phenomena in dissipative systems characterized by topological winding numbers have been studied in [9,10]. The Su-Schrieffer-Heeger (SSH) model originally used to describe the transport properties of conducting polyacetylene [11,12] has attracted increasing attention due to its simplest topological insulator model with a simple structure but rich physical pictures [9,13–15]. The SSH chain and its various extensions have been investigated in quantum state transfer [16–21] and topological transmission device constructions such as topological beam splitters and topological routers [22–25].

Waveguide quantum electrodynamic systems involving the coupling of atoms and one-dimensional propagation fields have become important physical platforms for realizing quantum information processing [26–35] and quantum simulation [36–39]. If the waveguide is designed with finite bandwidths, the physics of light-matter interactions in one dimension becomes complicated and interesting such as with coupled cavity arrays described by the tight-binding model [40,41] and one-dimensional topological photonic lattices described by the SSH model. When the transition frequency of the atom is located in the photonic band gap, the photons in the waveguide are localized around the atom, which forms the atom-photon bound state, and the overlap in the spatial distribution of the photons can mediate the coherent interactions between the atoms [42–45]. The interactions between atoms and waveguide result in many interesting phenomena and applications such as the generation of long-range atom entanglement [46,47], chiral interaction [48,49], and the simulation of topological states [50–52]. Particularly, when the atom couples to the topological waveguide with the periodic boundary, both the atom and photons behave in exotic ways called unconventional quantum optics [33,48,49,53,54]. For example, the atom can be viewed as an effective boundary and induce chiral zero-energy modes exhibiting a distribution of chirality as well as robustness to off-diagonal disorder.

However, little attention has been paid to atom coupling to finite-size topological waveguides. In this paper, considering the atom coupling to the finite SSH chain, we aim to control quantum information transmission by manipulating the atom. When the SSH chain is in the trivial phase, a bound state is formed, consisting of the atom in the excited state and localized waveguide photons, which cannot be used to transfer information between the atom and the chain. For the system in the topological phase, when the frequency of the atom is resonant with the center frequency of the SSH chain, an effective transition between the atomic excited state and the band-gap states can be obtained. Under the weak-coupling condition, the system can be equivalently described by the three-state model consisting of atomic excited states and band-gap states. In this case, the three-state model exists with a zero-energy state, allowing us to transfer the excitation of the atoms to the ends of the chain by adiabatically adjusting the parameters. And the transfer of excitation to the leftmost or rightmost ends of the chain depends on which sublattice of the cell the atom is coupled to. Moreover, we can also realize the transfer of excitation of the atom to the left or right edges states with dynamical evolution.

II. ATOM COUPLING WITH THE FINITE SSH CHAIN

We consider an atom coupled to a finite SSH chain at the pth cell of either sublattice A_p or sublattice B_p with the coupling strength g shown in Fig. 1. The total Hamiltonian

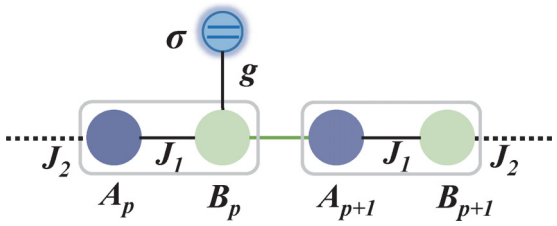

FIG. 1. Schematic illustration of the atom coupling to the finite SSH chains at sublattice B_p with coupling strength g. Alternately, the atom also can be coupled to the sublattice A_p (not shown here).

can be written as

$$H = H_{\rm SSH} + H_I + \omega_e \sigma^\dagger \sigma, \tag{1}$$

with

$$H_I = g c_p^\dagger \sigma + \text{H.c.}, \tag{2a}$$

$$H_{\rm SSH} = \sum_{i=1}^{N} \omega_o (a_i^\dagger a_i + b_i^\dagger b_i) + (J_1 a_i^\dagger b_i + J_2 a_{i+1}^\dagger b_i + \text{H.c.}). \tag{2b}$$

H_I represents the interaction between the atom and the SSH chain, where $c_p = \{a_p, b_p\}$. The Hamiltonian of the SSH chain described in Eq. (2b) is a one-dimensional lattice model with a hopping period of 2. Each cell of the lattice contains two sublattices A and B with frequencies ω_o. The intercell and extra-cell couplings are $J_1 = J(1+\cos\theta)$ and $J_2 = J(1-\cos\theta)$ with $\theta \in [0, 2\pi]$, respectively. Strictly speaking, the free terms in $H_{\rm SSH}$ partly break chiral symmetry of a standard SSH chain [4,13], but the quantized Zak phase remains as long as the frequency of each site is not perturbed [55,56]. We will use the center frequency of the SSH chain ω_o as the reference energy in the following discussion.

In the single-excited space, we label $|A_i\rangle = a_i^\dagger |G\rangle$ and $|B_i\rangle = b_i^\dagger |G\rangle$, where $|G\rangle$ is the ground state of the SSH chain. The Hamiltonian (2b) in single-excited space can be written as $H_{\rm SSH} = \sum_{i=1}^{N} \omega_o (|A_i\rangle\langle A_i| + |B_i\rangle\langle B_i|) + (J_1 |A_i\rangle\langle B_i| + J_2 |A_{i+1}\rangle\langle B_i| + \text{H.c.})$. We can diagonalize the Hamiltonian as $H_{\rm SSH} = \sum_{j=1}^{2N} E_j |\Psi_j\rangle\langle\Psi_j|$, where E_j and $|\Psi_j\rangle$ are the eigenenergies and eigenvectors. $|\Psi_j\rangle$ can be written as the superposition of $|A_i\rangle$ and $|B_i\rangle$ as $|\Psi_j\rangle = \sum_{i=1}^{N} (\zeta_{2i-1,j} |A_i\rangle + \zeta_{2i,j} |B_i\rangle)$, where $\zeta_{2i-1,j} = \langle A_i|\Psi_j\rangle$ and $\zeta_{2i,j} = \langle B_i|\Psi_j\rangle$ are the projections of the eigenvectors on the sublattice A_i and B_i. Conversely the basis $|A_i\rangle$ and $|B_i\rangle$ can also be written as the superposition of the eigenvectors as $|A_i\rangle = \sum_{j=1}^{N} \zeta_{2i-1,j}^* |\Psi_j\rangle$ and $|B_i\rangle = \sum_{j=1}^{N} \zeta_{2i,j}^* |\Psi_j\rangle$.

In Fig. 2(a), we plot the energy spectrum varying with θ under open boundary condition. It can be seen that the SSH chain possesses two band-gap states $|\Psi_N\rangle$ and $|\Psi_{N+1}\rangle$ in the gap $\theta \in [0.5\pi, 1.5\pi]$ (topological phase). The probability distribution of the band-gap states $|\Psi_N\rangle$ varies with θ shown in Fig. 2(b). It is clear that the band-gap states are mainly located at the two ends of the chain with the same probability. The energy of the two band-gap states can be obtained as $E_N = -E_{N+1} = (-1)^{N+1} N_L^2 J_1 (J_1/J_2)^{N-1}$ and

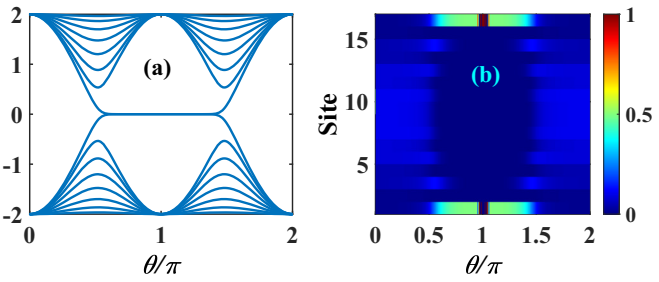

FIG. 2. (a) The energy spectrum of the SSH chain varies with the variation of θ. (b) The probability distribution of the eigenstates corresponds to panel (a). The parameters are $N = 8$ and $J = 1$.

the corresponding wave function can be written as

$$|\Psi_N\rangle = \frac{1}{\sqrt{2}}(|\psi_L\rangle + |\psi_R\rangle),$$
$$|\Psi_{N+1}\rangle = \frac{1}{\sqrt{2}}(|\psi_L\rangle - |\psi_R\rangle), \tag{3}$$

where $|\psi_L\rangle = N_L \sum_{i=1}^{N} c_i^a |A_i\rangle$ and $|\psi_R\rangle = N_R \sum_{i=1}^{N} c_i^b |B_i\rangle$ are the left and right edge states with $c_i^a = (-\frac{J_1}{J_2})^{i-1}$, $c_i^b = (-\frac{J_1}{J_2})^{N-i}$ and the normalization factors $N_L = N_R = [1-(J_1/J_2)^2]^{1/2}[1-(J_1/J_2)^{2N}]^{-1/2}$. Therefore, we can obtain $\zeta_{2i-1,N} = \zeta_{2i-1,N+1} = N_L c_i^a$ and $\zeta_{2i,N} = -\zeta_{2i,N+1} = N_R c_i^b$. When the atom couples the sublattice B_p, the total Hamiltonian can be rewritten as

$$H = \Delta \sigma^\dagger \sigma + \sum_{j=1}^{2N} [E_j |\Psi_j\rangle\langle\Psi_j| + (g\zeta_{2p,j}^* \Psi_j^\dagger \sigma + \text{H.c.})], \tag{4}$$

where $\Delta = \omega_e - \omega_o$ is the detuning between the atom and the center frequency of the SSH chain and $\Psi_j^\dagger = |\Psi_j\rangle\langle G|$.

In Fig. 3(a), we plot the energy spectrum of the Hamiltonian (1) in the reference frequency ω_a varying with Δ for the chain in the trivial phase with $\theta = 0.4\pi$. We focus on the atomic frequency falling within the middle band gap, for other cases not discussed here. It can be seen that the energy in the range of $[-2J, -0.69J]$ and $[0.69J, 2J]$ is the scatter states and the energy in $[-0.69J, 0.69J]$ is the atom-photon bound state. When $\Delta = 0 \in [-0.69J, 0.69J]$, $\theta = 0.4\pi$ (trivial phase), we plot the dynamic of the system varying with time under the initial state of the system in the atomic excited state as shown in Fig. 3(b). We can see that the excitation remains in the atom and is not exchanged with the SSH chain. Meanwhile, in the inset of Fig. 3(b), we display the distribution of the SSH chain photons on the site. It can be clearly seen that the photon is localized only exponentially on the left sublattice A of the atom, which is called the photon bound state. This phenomenon is similar to the atom coupling with the SSH chain under periodic boundary condition [48] and the emission of the photon from the atom to the SSH chain is prohibited.

For the atom coupling to the finite SSH chain in the topological phase ($\theta = 0.65\pi$), the energy spectrum is shown in Fig. 3(c), and the enlargement at the region $\Delta \in [-0.05, 0.05]$ is displayed in Fig. 3(e). We can see that when $\Delta = 0$ the energy levels of band-gap states exhibit anticrossover

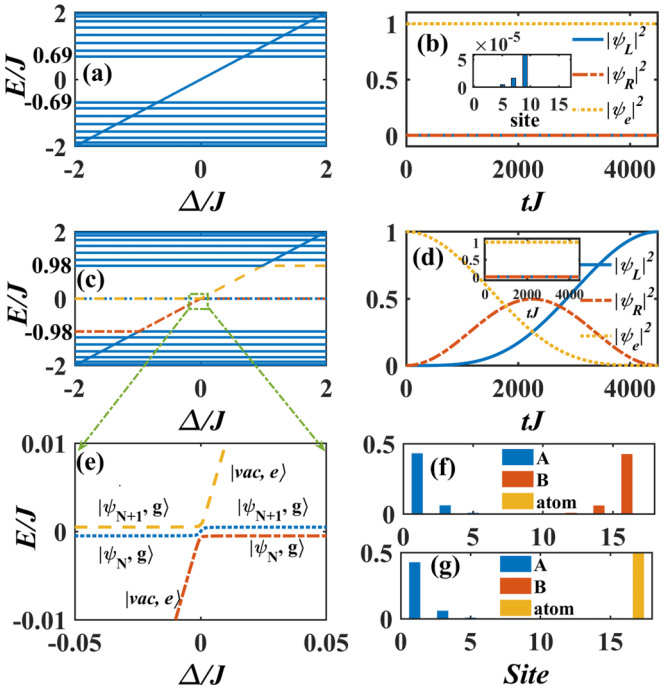

FIG. 3. [(a), (c)] The energy spectrum of the system vs Δ for the SSH chain in the (a) trivial phase $\theta = 0.4\pi$ and (c) topological phase $\theta = 0.65\pi$. (b) The probability evolution of the atomic excited state $|\psi_e|^2$, left edge state $|\psi_L|^2$, and right edge state $|\psi_R|^2$ with $\Delta = 0$ and $\theta = 0.4\pi$ (trivial phase), where the inset displays the probability of the waveguide photons on the sites. (d) The probability of $|\psi_e|^2$, $|\psi_L|^2$, and $|\psi_R|^2$ with $\Delta = 0$ for $\Delta = 0.04J$ in the inset. (e) The enlargement of panel (c) in the region $\Delta \in [-0.05, 0.05]$. [(f), (g)] The probability distribution of band-gap states corresponding to the blue dotted line in panel (e) for (f) $\Delta = 0.04J$ and (g) $\Delta = 0$. For panels [(d)–(g)], the parameter $\theta = 0.65\pi$ (topological phase), and the other parameters are $p = 5$, $N = 8$, $g = 0.01J$, and $J = 1$.

behavior. When the detuning is far away from the resonance the energy levels are separated from each other. In Figs. 3(f) and 3(g), we plot the probability distribution of band-gap states corresponding to the blue dotted line in Fig. 3(e) for $\Delta = 0.04J$ and 0, respectively. It can be seen that the probability distribution of the band-gap state distributes only on the chain when $\Delta = 0.04J$. However, when $\Delta = 0$, the probability distribution of the band-gap states is distributed over both atom and SSH chain as shown in Fig. 3(g), which implies that the band-gap state is hybridized. For the detuning far away from the resonance, the main components of these band-gap states are labeled in Fig. 3(e), where $|\psi_{N(N+1)}, g\rangle$ ($|\text{vac}, e\rangle$) denotes that the SSH chain is in the state $|\psi_{N(N+1)}\rangle$ (in the vacuum state) and the atom is in the ground state $|g\rangle$ (in the excited state $|e\rangle$). The dynamics evolution of the system with time for the atom initially in the excited state was plotted in Fig. 3(d) for $\Delta = 0.04J$ and 0. We can find that the effective transitions between the atomic excited state and band-gap states are prohibited when $\Delta = 0.04J$ as seen in the inset of Fig. 3(d). When $\Delta = 0$, we can see the exchanges between the atomic excited state and two edge states, which means the effective coupling between the band-gap states and the atomic excited state. In addition, as displayed in Fig. 3(e), in the topological phase, if we adiabatically tune Δ to resonate with the edge mode $|\Phi_N\rangle$ or $|\Phi_{N+1}\rangle$, then the atomic excitations are converted to $|L\rangle + |R\rangle$ or $|L\rangle - |R\rangle$, thus generating long-distance quantum entanglement at both ends. In conclusion, in the topological phase, when the atomic frequency is resonant with the center frequency of the SSH chain, i.e., $\Delta = 0$, an effective transition between the excited state of the atom $|\text{vac}, e\rangle$ and the band-gap state $|\psi_{N(N+1)}, g\rangle$ occurs, while in any other cases the atom cannot exchange the excitation with the SSH chain.

Next, we consider the atom resonantly interacting with the SSH chain with $\Delta = 0$. Under the condition $g/J \ll 1$, due to the energy of band-gap states with $E_{N(N+1)} \approx 0$, which is near resonant with the atomic frequency, the coupling between other eigenstates and the atom can be ignored due to $|E_j|_{Mix} = |E_{N-1(N+2)} \gg g\zeta^*_{2p,j}$. In a word, the atom only couples with the two energy levels $|\Psi_N\rangle$ and $|\Psi_{N+1}\rangle$. Thus when the atom couples to sublattice B_p, the effective Hamiltonian can be written as

$$H = E_N \Psi_N^\dagger \Psi_N + E_{N+1} \Psi_{N+1}^\dagger \Psi_{N+1} + N_L g c_p^b / \sqrt{2} (\Psi_N^\dagger - \Psi_{N+1}^\dagger)\sigma + \text{H.c.} \quad (5)$$

Therefore, in single-excitation space, when we consider the frequency of the atom as resonant with the SSH chain, the above Hamiltonian only causes the subspace transitions $|\psi_N, g\rangle \leftrightarrow |\text{vac}, e\rangle \leftrightarrow |\psi_{N+1}, g\rangle$. The case of the atom coupling to sublattice A_p can also be analyzed similarly, but we will not go into details. During the review process of this paper, we read the recent work [57], which also investigated atom coupling with a finite SSH chain leading to a coupling-dependent hybridization of the atomic and edge states, which in turn establishes a highly accurate three-state model equivalently describing the whole system. Different from [57], here we focus on how adiabatic processes can be used to realize the transfer of atomic excitations to the end of the chain, and the effect of the coupling position of the atoms on the excitation transfer.

III. CONTROLLABLE EXCITATION TRANSFER THROUGH THE ADIABATIC PROCESS

Because the band-gap states of the SSH chain can be written as the superposition of edge states as Eq. (3), when the atom couples with the SSH chain at sublattice B_p, the effective transition between the band-gap states and the atomic excited state Eq. (5) can be rewritten in the subspace $\{|\text{vac}, e\rangle, |\psi_L, g\rangle, |\psi_R, g\rangle\}$:

$$H_{\text{sub}} = G|\psi_L, g\rangle\langle\psi_R, g| + G_{R,b}|\psi_R, g\rangle\langle\text{vac}, e| + \text{H.c.}, \quad (6)$$

where we set $G = E_N = (-1)^{N+1} N_L^2 J_1 (J_1/J_2)^{N-1}$, and $G_{R,b} = g N_L (-\frac{J_1}{J_2})^{N-p}$. We can find that when the atom is coupled to sublattice B_p the atom is equivalently coupled to the right edge state. Due to finite-size effects, the right edge state is coupled to the left edge state. In this case, the three-state model can be viewed as a "Λ" configuration $|\text{vac}, e\rangle \longleftrightarrow |\psi_R, g\rangle \longleftrightarrow$

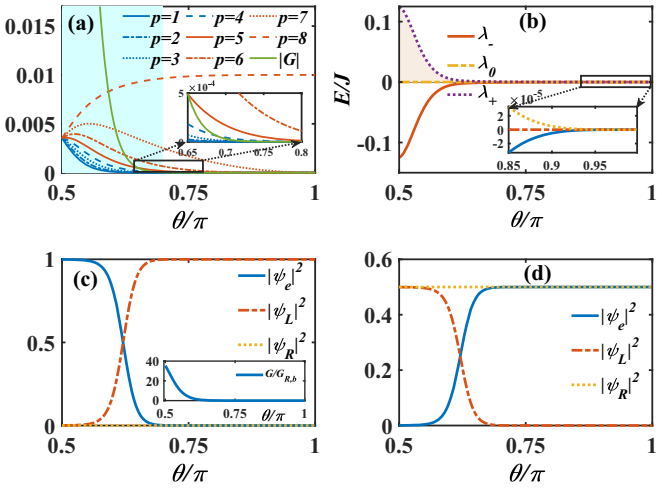

FIG. 4. (a) The parameters $|G|$ and $|G_{R,b}|$ as a function of θ for different p. (b) The eigenenergies vary with θ for $p = 6$. [(c), (d)] Distribution of the probability of eigenstates in excited-state atoms and left and right edge states of (c) $|\phi_0\rangle$ and (d) $|\phi_+\rangle$ for $p = 6$. The parameters are $N = 8$, $g = 0.01J$, $\Delta = 0$, and $J = 1$.

$|\psi_L, g\rangle$. Rewriting Eq. (6) in the matrix form, we can obtain

$$H_{\text{sub}} = \begin{bmatrix} 0 & 0 & G_{R,b} \\ 0 & 0 & G \\ G_{R,b} & G & 0 \end{bmatrix}. \tag{7}$$

The eigenvalues of H_{sub} can be obtained by solving the cubic equation

$$\lambda^3 - \left(G^2 + G_{R,b}^2\right)\lambda = 0. \tag{8}$$

The eigenenergies of Eq. (8) can be solved as $\lambda_{0(\pm)} = 0, \pm\sqrt{G^2 + G_{R,b}^2}$. The corresponding eigenstates can be obtained as $|\phi_0\rangle = \{\cos\nu; \sin\nu; 0\}$, $|\phi_\pm\rangle = N_\pm\{\pm\frac{G_{R,b}}{\sqrt{G^2+G_{R,b}^2}}, \pm\frac{G}{\sqrt{G^2+G_{R,b}^2}}, 1\}$, where $N_\pm$ is the normalization coefficient and $\nu = \arctan(G_{R,b}/G)$. It can be seen that for the zero-energy eigenstate $|\phi_0\rangle$ is a superposition of the atom excited state with probability $\cos^2\nu$ and the left edge state with probability $\sin^2\nu$. If we slowly adiabatically tune θ from 0.5π to π, the parameter ν changes from 0 to $\pi/2$ corresponding to the parameter changing from $G_{R,b}/G \ll 1$ to $G_{R,b}/G \gg 1$, and then the zero-energy eigenstate adiabatically evolves from $|\phi_0\rangle = \{1; 0; 0\}$ to $\{0; 1; 0\}$. During slow change of θ from $\pi/2$ to π, the probability of the left edge state $|\psi_L\rangle$ is mainly distributed on the left sublattice A_i, and will eventually be fully distributed on the leftmost sublattice A_1 (for details see the Appendix), under a certain group of parameters. Actually, the zero-energy eigenstate $|\phi_0\rangle$ is the so-called dark state or coherent population trapping state and the adiabatic evolution of the zero-energy state analogous to the stimulated Raman adiabatic passage process [58].

In Fig. 4(a), we plot the parameters G and $G_{R,b}$ varying θ for different coupling positions p for $N = 8$. We can observe that, for $p < 5$, G is always greater than $G_{R,b}$ and, for $p \geqslant 5$, G changes from greater than $G_{R,b}$ to less than $G_{R,b}$. When $\theta > 0.7\pi$, $G < 10^{-6}$ is converging to zero and $G_{R,b} > G$ for only $p \geqslant 5$ [see inset in Fig. 4(a)]. In Fig. 4(b), we plot the eigenenergies $\lambda_\pm$ and λ_0 varying with θ for $p = 6$. We can see that the eigenenergies $\lambda_\pm$ will tend to zero ($|\lambda_\pm| < 10^{-6}$) when $\theta > 0.95\pi$, leading to the near degeneracy of the three energy levels and the invalidity of the adiabatic passage. We can understand the requirement for $p \geqslant 5$ and the range of θ from the condition of the adiabatic process, which demands that the time rate of the equivalent interaction $\dot{\nu}$ is less than the difference between the instantaneous eigenenergies $\Delta_\lambda = \sqrt{G^2 + G_{R,b}^2}$ [59]; thus the energy-level difference should be nonzero, i.e., $\Delta_\lambda > 0$, until the excitation is transferred. This condition results in the requirement $p \geqslant 5$ and the range of θ. In addition, we can use global adiabatic conditions to discuss the requirement for the parameters (the details are given in the Appendix). The global adiabatic condition yields the same result as the nonzero band-gap condition, both of which require $p \geqslant 5$. We must point out that $p \geqslant 5$ and the range of θ in Fig. 4(b) is only valid for $N = 8$. If N is different, the requirement for the value of p and θ under the adiabatic condition is different because $\Delta_\lambda > 0$ relates with N and g [see Eq. (A2)], which means that one can use the adiabatic condition to find a reasonable value p and θ for certain N.

In Fig. 4(c), we plot the probability of the atom $|\psi_e|^2$, $|\psi_L|^2$, and $|\psi_R|^2$ as a function of θ for $|\phi_0\rangle$. We find that, when $\theta = 0.5\pi$ and $G/G_{R,b} \gg 1$, $|\phi_0\rangle$ is mainly concentrated on the atomic excited state; with increasing θ, $G/G_{R,b} \to 0$ and $|\phi_0\rangle$ is most concentrated on the left edge state as presented in Fig. 4(c). Thus, by adiabatically tuning θ, we can realize the transfer of atomic excitation to the left edge state. For $|\phi_+\rangle$, it is transferred to the excited state of the atom and right edge states with the same probability when $\theta \to \pi$ as shown in Fig. 4(d). Similarly, when the atom is coupled to the sublattice A_p, there is still an eigenstate with zero eigenvalue, $|\phi_0\rangle = \{-G/G_{L,a}, 0, 1\}$, where $G_{L,a}$ is the transition between the atomic excited state and the left edge state. It can be found that $|\phi_0\rangle$ is a superposition of the atomic excited state and the right edge state. By adjusting θ, we can find that, as θ increases, the excitation is distributed mainly in the atomic excited state initially and the excitation is transferred to the right edge state finally. In addition, it is worth noting that, when $\theta = \pi$, the left (right) edge states are mainly distributed on the leftmost (rightmost) sublattice A_1 (B_{2N}), which implies that the atom in the excited state can be transferred to the end of the chain through SSH mode channels, and the direction is completely controllable by setting the atom coupling to sublattice A_p or B_p. In a word, when the atom couples to B_p, the excitation of the atom is transferred to A_1; if the atom couples to A_p, the excitation of the atom is transferred to B_N. This unidirectional transition is resulted from hybridization of the edge states for the finite-size chain and related to the topology property of the chain.

In order to prove the correctness of the three-state model, in Fig. 5(a), we plot the energy spectrum varying θ under the case where the atom couples to sublattice B_p for the total Hamiltonian (1). It can be seen that there are three band-gap states, where a zero-energy state $|E_{N+1}\rangle$ is in all ranges and $|E_N\rangle$ and $|E_{N+2}\rangle$ are in $\theta \in [0.5\pi, \pi]$. In order to investigate the zero-energy state $|E_{N+1}\rangle$, we plot the probability distribution of $|E_{N+1}\rangle$ on the sites varying θ as shown in Fig. 5(c). We find that in the range $\theta \in [0, 0.5\pi]$ the probability distribution of $|E_{N+1}\rangle$ is concentrated on the atom, and it gradually

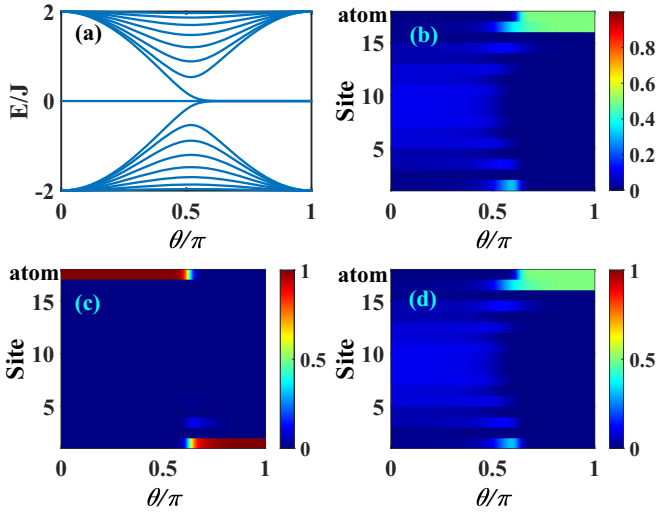

FIG. 5. (a) The energy spectrum with the variation of θ when the small atom couples with sublattice B. [(b), (c), (d)] The probability distribution of the three band-gap states $|E_N\rangle$, $|E_{N+1}\rangle$, and $|E_{N+2}\rangle$, respectively, on the sites varies with θ. The parameters are $N = 8$, $g = 0.01J$, $p = 6$, and $J = 1$.

transfers to the rightmost sublattice A_1 as θ increases. We have also investigated the distribution of the probability of the other band-gap states as shown in Figs. 5(b) and 5(d). It can be found that the distribution of the band-gap states is mainly concentrated on the excited state of the atom and right edge states with the SSH chain in the topological phase, which is consistent with $|\phi_{\pm}\rangle$. That indicates that our previous discussion in the subspace is reasonable. The above results mean that we can realize controlled quantum information transfer. The atom acts as the transmitter of the signal and the ends of the chain (A_1, B_{2N}) act as the receiver of the information. The transfer of information to the leftmost or rightmost ends of the chain is achieved by controlling the atom coupling to sublattice A_p or B_p, respectively.

Now, under a slowly time varying rate, we directly employ time-dependent Hamiltonian (1) to prove the correction of the above discussion. We set $\theta = \Omega t$, Ω is the slowly time varying rate, the atom is initially in the excited state, and the topological chain is in the vacuum state so $|\psi_i\rangle = |0, 0, \ldots, 0, 1\rangle$.

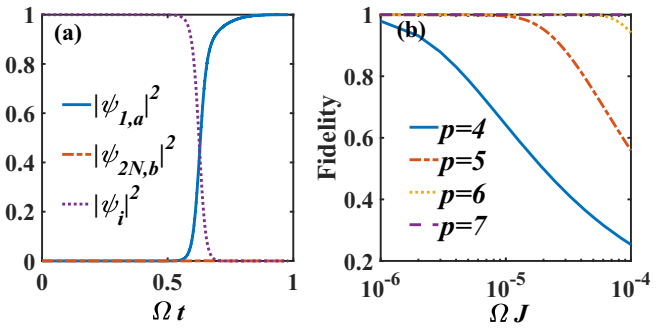

FIG. 6. (a) The probability evolution with time for the atom coupling with sublattice B with $p = 6$, $N = 8$, and $\Omega = 10^{-5}J$. (b) The evolution of fidelity F for different coupling positions $p = 4, 5, 6, 8$. The parameters are $g = 0.01J$ and $J = 1$.

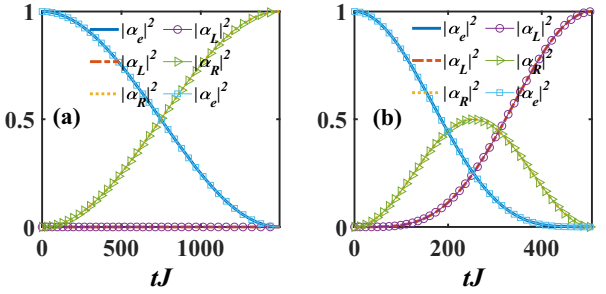

FIG. 7. The probability of the excited atom $|\alpha_e(t)|^2$ and the right and left edge states $|\alpha_{R,L}(t)|^2$ varying with time for (a) $\theta = 0.8\pi$ and (b) $\theta = 0.6057\pi$. The other parameters are $g = 0.01J$, $p = 7, N = 8$, $\Delta = 0$, and $J = 1$.

With Schrödinger equation $i\frac{d|\Psi\rangle}{dt} = H|\Psi\rangle$, we can derive the final state $|\psi_f\rangle$. The results of the numerical simulations are displayed in Fig. 6(a), where $|\psi_{1,a}|^2$ and $|\psi_{2N,b}|^2$ are the probability of the leftmost and rightmost sublattices, respectively. It can be seen that when the atom couples to sublattice B_p the excitation is transferred to the leftmost sublattice A_1, which is consistent with Fig. 5(c). Meanwhile, when the atom couples to sublattice A_p, the excitation is transferred to the rightmost sublattice B_{2N}; the latter case is not shown here. However, during the evolution, the parameter θ needs to be adiabatically varied to ensure a sufficiently high probability of success [20,25]. In Fig. 6(b), we plot the fidelity $F = \langle\psi_t|\psi_f\rangle$ at time $t_f = \pi/\Omega$ varying Ω for different coupling positions p, where $|\psi_t\rangle = |1, 0, \ldots, 0, 0\rangle$ is the target state. The numerical results show that for a fixed Ω, e.g., $\Omega = 10^{-5}J$, the fidelity is very low for $p < 5$ and the fidelity can reach 1 for $p \geqslant 5$. This arises from the fact that the band gap $\Delta_\lambda = \sqrt{G^2 + G_{R,b}^2}$ increases with p, which is more favorable for the adiabatic condition. With Ω increasing to $\Omega = 10^{-4}J$, even if $p = 6$, the fidelity still does not reach 1. For $p = 7, 8$, the fidelity can reach 1 for $\Omega \in [10^{-6}J, 10^{-4}J]$. The above results are consistent with the adiabatic condition parameter requirements in Fig. 10. In a word, as the atom approaches closer to the leftmost sublattice B_{2N} with a larger value of p, the time varying rate Ω can be relaxed to some degree.

IV. EXCITATION TRANSFER WITH DYNAMIC EVOLUTION

In this section, we discuss the controllable excitation transfer beyond the adiabatic process. In [57], it is mentioned that controlled excitation transfer can also be realized by considering the different coupling strengths of the atoms to the SSH chains; for weak coupling strength, the excitation of the atoms can be transferred to both sides of the chain, and for strong coupling strength it will result in the transfer of the atomic excitation to one side of the chain. Here we focus on the effect of the dimerization strength (θ) of the SSH chain on the excitation transfer, and the results show that we can set different dimerization strengths to achieve atomic excitation transfer to either side of the chain. We take the atom coupling sublattice B_p as an example. In the topological phase, when the atom is in the excited state initially, under the Hamiltonian

(7), the state will evolve as

$$|\psi(t)\rangle = \alpha_e(t)|\text{vac}, e\rangle + \alpha_L(t)|\psi_L, g\rangle + \alpha_R(t)|\psi_R, g\rangle, \quad (9)$$

with

$$\alpha_e(t) = \frac{G^2 + G_{R,b}^2 \cos\left[\sqrt{G^2 + G_{R,b}^2}t\right]}{G^2 + G_{R,b}^2},$$

$$\alpha_L(t) = \frac{-GG_{R,b} + GG_{R,b}\cos\left[\sqrt{G^2 + G_{R,b}^2}t\right]}{G^2 + G_{R,b}^2},$$

$$\alpha_R(t) = \frac{iG_{R,b}\sin\left[\sqrt{G^2 + G_{R,b}^2}t\right]}{\sqrt{G^2 + G_{R,b}^2}}. \quad (10)$$

Apparently, the above probability amplitudes depend on G and $G_{R,b}$. As shown in Fig. 4(a), when $\theta \approx 0.73\pi$ and $G \approx 0$, thus the probability amplitude of left edge state $\alpha_L(t) = 0$, the atom and the right edge state exhibit Rabi oscillations with the period depending on $G_{R,b}$. The result is displayed in Fig. 7(a), where the marker (circle, triangle and square) lines represent the results from solving the full Hamiltonian Eq. (1) dynamics evolution and the others are obtained by Eq. (10). For $0.5\pi < \theta < 0.7\pi$ and $p = 7$, we find when $\theta = 0.6057\pi$ and $G = G_{R,b}$ that the amplitudes become $\alpha_e(t) = [1 + \cos(\sqrt{2}Gt)]/2$, $\alpha_L(t) = [-1 + \cos(\sqrt{2}Gt)]/2$, and $\alpha_R(t) = i\sin(\sqrt{2}Gt)/\sqrt{2}$. It is evident that as t varies from 0 to $\pi/(\sqrt{2}G)$ the excitation is distinctly transferred from the atom to the left edge state, as illustrated in Fig. 7(b). In addition, when $t_f = \pi/\sqrt{G^2 + G_{R,b}^2}$ and $\alpha_R(t_f) = 0$, in this time $|\psi(t_f)\rangle$ is a superposition of the excited atomic state and the left edge state as $|\psi(t_f)\rangle = (\frac{G^2 - G_{R,b}^2}{G^2 + G_{R,b}^2}|10\rangle + \frac{-2GG_{R,b}}{G^2 + G_{R,b}^2}|01\rangle)|0_R\rangle$. Thus, by setting the coupling point and θ, we can achieve the excitation transferred from the atom to the ends of the chain under the dynamic evolution.

V. SSH CHAIN-COUPLED DISORDER AND ATOMIC MISMATCH FREQUENCY EFFECTS ON EXCITATION TRANSFER

Next, we discuss the effects of disorder on the energy spectrum and the probability of distribution of the band-gap state, where we mainly consider the effect of diagonal and off-diagonal disorder. Taking disorder perturbations into consideration, the Hamiltonian (1) becomes

$$H = \Delta\sigma^\dagger\sigma + \sum_{i=1}^{N} \varepsilon a_i^\dagger a_i + \varepsilon b_i^\dagger b_i + (g a_p^\dagger \sigma + \text{H.c.}) + \sum_{i=1}^{N}[(J_1 + \eta)a_i^\dagger b_i + (J_2 + \eta)a_{i+1}^\dagger b_i + \text{H.c.}], \quad (11)$$

where ε and η are the diagonal and off-diagonal disorder and the atom couples to the sublattice A_p. We consider ε and η to be random numbers in the range $[-\xi, \xi]$, where ξ is the disorder strength. In Figs. 8(a) and 8(c), we plot the energy spectrum varying θ under the off-diagonal disorder ($\varepsilon = 0$) with strength $\xi = 0.1J$ and $0.5J$, respectively. It can be seen that the presence of disorder affects the energy spectrum, but the energy of the band-gap state marked by the orange dashed line is not affected. For weak off-diagonal disorder, the probability distribution of the band-gap state marked by the orange dashed line is not influenced, but it is obviously affected for the larger disorder strength comparing Figs. 8(b) and 8(d). For diagonal disorder ($\eta = 0$), we find that the energy of the band-gap state is not sensitive but the probability distribution of the band-gap state is very sensitive as shown in Figs. 8(e) and 8(f).

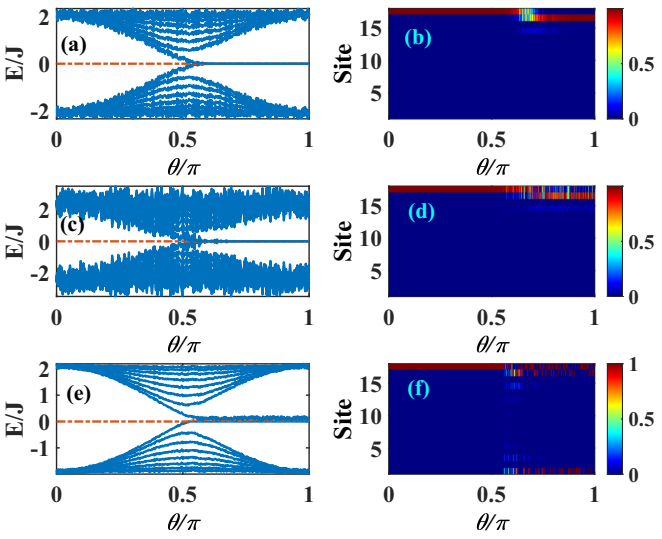

FIG. 8. [(a), (c), (e)] The energy spectrum varies with θ for the disorder within the region (a) $\eta \in [-0.1J, 0.1J]$, $\varepsilon = 0$; (c) $\eta \in [-0.5J, 0.5J]$, $\varepsilon = 0$; and (e) $\eta = 0$, $\varepsilon \in [-0.1J, 0.1J]$. [(b), (d), (f)] The probability of distribution of the band-gap state varies with θ corresponding to the orange dashed line in panels (a), (c), and (e). The parameters are $g = 0.01J$, $N = 8$, $p = 6$, $\Delta = 0$, and $J = 1$.

In Sec. III, we investigate atom resonance coupling to the SSH chain $\Delta = 0$, and the case of frequency mismatch $\Delta \neq 0$ should be discussed. Considering this case is meaningful, e.g., in superconducting circuits experiments; in order to realize $\Delta = 0$, a tunable quantum qubit is usually required; however, the tunable quantum qubit is affected by decoherence noise, which in turn produces a change in frequency [60]. In Fig. 9, we plot the evolution of fidelity varying with Δ. We can see that for $|\Delta| < 0.05J$ the fidelity can be greater than 95% but the fidelity decreases rapidly as Δ continues to increase. This is due to the fact that when the detuning value is large the atoms no longer resonate with the band-gap state of the SSH

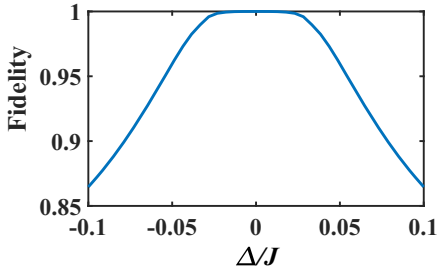

FIG. 9. The fidelity at $t = \pi/\Omega$ as a function of Δ with $N = 8$, $\Omega = 10^{-5}J$, and $p = 6$. The parameters are $g = 0.01J$ and $J = 1$.

chain, and therefore the fidelity decreases rapidly. Thus, for the present model, it is immune to weak off-diagonal disorder and slight mismatch frequency.

VI. DISCUSSION

For an odd number of sites in the SSH chain, there will always be a zero-energy edge state $|\phi\rangle$ in the energy spectrum band gap. When atomic resonances are coupled to the SSH chain, the system can be approximated to a subspace $\{|\phi, g\rangle, |\text{vac}, e\rangle\}$ consisting of the zero-energy state and atomic excited states. Under this case, the eigenenergies and corresponding eigenstates $E_\pm = \pm G_0$ and $\phi_\pm = 1/\sqrt{2}\{1; \pm 1\}$, where G_0 is the coupling between the zero-energy state and atomic excited state. Obviously this is a superposition of the zero-energy state and the excited state of the atom and has the same probability. As a result, we could not realize the transfer of atomic excitations to the end of the chain through an adiabatic process.

Next, we discuss the experimental feasibility. In recent years, based on the flexibility of the parameters and the design capability of the system structure [61,62], superconducting circuits have attracted much attention and have evolved into well-established platforms for the study of quantum simulation [63–65], quantum computation [66], and quantum information processing [67,68]. Recently, these works [38,48,69] have pointed out theoretically and experimentally that each cell of the SSH chain can be mapped to the two *LC* resonators. The relative magnitude of intra- and intercell coupling between neighboring resonators is determined by the auxiliary capacitance and inductance [70,71]. By designing the intra- and extra-cell capacitance and inductance, a periodic modulation of the coupling can be achieved to obtain the SSH chain. Because of the inevitable loss of atoms in real systems, the time t_f to complete the transfer of excitation from the atom to the leftmost sublattice A_1 needs to be much larger than the decoherence time of the atom during the state transfer process. Recently, coherence times of the order of millimeters ($t \approx 10^{-3}$ s) for superconducting bits have been realized based on state-of-the-art experimental systems [72]. As mentioned in Fig. 6(b), when $p = 5$, we only need $\Omega = 10^{-5}J$ to achieve high-fidelity excitation transfer. The time to complete the transfer of the adiabatic state $t_f = \pi/(\Omega J)$. In [38], the unit coupling strength of the SSH chain $J \approx 10^8$Hz, thus the time $t_f = 10^{-3}$ s approximately equals to the state-of-the-art atomic decoherence time. Since the adiabatic requirement Ω becomes progressively larger as p increases [shown in Fig. 10(c)], for example, if $q = 7$, we only need $\Omega = 10^{-4}J$, which corresponds to a time of excitation transfer $t_f = 10^{-4}$ s much smaller than the decoherence time of the atoms. Therefore, our scheme may be realized in superconducting circuits.

VII. CONCLUSION

In this paper, we study the coupling of an atom with a finite-size SSH chain and aim to realize the controllable excitation transfer between the atom and the ends of the SSH chain. In the topological phase, when the frequency of the atom is resonant with the center frequency of the SSH chain, an effective transition between the atomic excited state and the band-gap states can be observed. Under weak-coupling conditions, the system can be equated to a three-state model, consisting of an atomic excited state and two band-gap states. By solving the eigenvalues of the three-state system, we find that there exists a zero-energy state, and we can use adiabatic processes to adjust the probability distribution of the zero-energy state. In turn, we can transfer the excitation of the atom to one of the ends of the SSH chain, and which end they are transferred to depends on which sublattice of the cell the atom is coupled to. Furthermore, the excitation can also be transferred from the atom to the ends of the chain by fixing the parameters under the dynamic evolution.

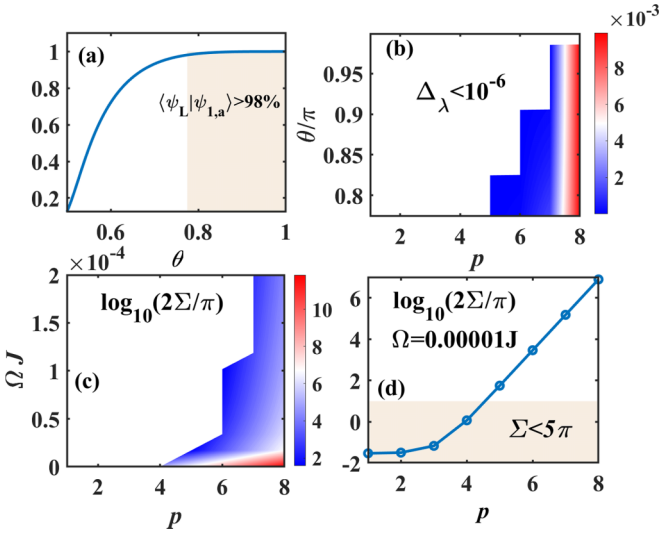

FIG. 10. (a) $F = \langle\psi_L|\psi_{1,a}\rangle$ varies with θ, where the fidelity reaching 98% means that the left edge state is completely concentrated in $|A_1\rangle$. (b) Δ_λ varies with Ω and p. The color region corresponds to $\Delta_\lambda > 10^{-6}$. (c) The area Σ varies with Ω and p. The color area denotes $\log(2\Sigma/\pi) > 0$. (d) The area Σ as a function of p for $\Omega = 0.000\,01J$. The parameters are $N = 8$, $g = 0.01J$, $\Delta = 0$, and $J = 1$.

ACKNOWLEDGMENTS

This work is supported by the National Natural Science Foundation of China under Grant No. 12274053 and National Key R&D Program of China (Grant No. 2021YFE0193500).

APPENDIX: ADIABATIC CONDITIONS

The adiabatic process requires that the time change rate of the equivalent interaction $\dot{\nu}$ is less than the difference between the instantaneous eigenenergies [59]. Corresponding to the current system, the adiabatic condition is

$$|\dot{\nu}| \ll \Delta_\lambda. \tag{A1}$$

Thus the energy-level difference should be nonzero until the excitation is transferred, i.e., $\Delta_\lambda > 0$, which can be satisfied by assuming $\Delta_\lambda > 10^{-6}$. Next we discuss how the distribution of the probability that the left edge state $|\psi_L\rangle$ is in the leftmost sublattice A_1 changes with θ as θ changes from $\pi/2$ to π. We use the fidelity $F = \langle\psi_L|\psi_{1,a}\rangle$ to indicate when

the left edge states are distributed in $|A_1\rangle$. The fidelity reaching 98% means that the left edge state is completely concentrated in $|A_1\rangle$. As shown in Fig. 10(a), when θ changes, F gradually increases, and when $\theta \geqslant 0.775\pi$ (orange region) $F > 98\%$ is always satisfied. Thus we just need to ensure that when $\theta > 0.775\pi$ then $\Delta_\lambda > 10^{-6}$, namely,

$$\sqrt{N_L^4 J_1 \left(-\frac{J_1}{J_2}\right)^{2N-2} + g^2 N_L^2 \left(-\frac{J_1}{J_2}\right)^{2N-2p}} > 10^{-6}. \quad \text{(A2)}$$

In Fig. 10(b), we plot $\Delta_\lambda > 10^{-6}$ corresponding the parameters region. We can see that $\Delta_\lambda > 10^{-6}$ is satisfied only if $p \geqslant 5$. By integrating Eq. (A1) over the interaction duration, we can obtain the global adiabatic conditions. The global adiabatic condition can be expressed as an area condition [58]:

$$\Sigma = \int_{t_i}^{t_f} dt \sqrt{G^2 + G_{R,b}^2} = \int_{t_i}^{t_f} dt \lambda_+(t) \gg \frac{\pi}{2}, \quad \text{(A3)}$$

where $t_i = \pi/(2\Omega)$ and $t_f = \pi/\Omega$. Obviously Σ corresponds to the area of the instantaneous eigenenergy λ_+ in the adiabatic evolution surrounded (below the purple dotted line) by the x axis as shown in Fig. 4(b) with the shadow region. When $\Omega t \in [0.5\pi, \pi]$, due to $J_1/J_2 < 1$, G and $G_{R,b}$ decrease power exponentially with increasing N for a fixed p, and then we need enough time to satisfy the global adiabatic conditions, namely, a sufficiently small Ω. When $J_1/J_2 < 1$, N and Ω are fixed, and the global adiabatic condition will be more fulfilled as the atomic positions approach closer to the end of the chain (the larger p is) since $G_{R,b}$ grows power exponentially with p. In Fig. 10(c), we plot the area conditions Σ varying with p and Ω for $N = 8$, where the color region denotes $\log(2\Sigma/\pi) > 1$, namely, the parameter zones where the adiabatic conditions are satisfied [73]. For different p, the rate of change is different to satisfy the adiabatic condition, but at least $p \geqslant 5$. For example, for $\Omega = 0.00001J$, the area increases gradually as p and the adiabatic condition is satisfied only when $p \geqslant 5$ as displayed in Fig. 10(d).

[1] M. Z. Hasan and C. L. Kane, *Colloquium*: Topological insulators, Rev. Mod. Phys. **82**, 3045 (2010).

[2] L. A. Wray, S. Y. Xu, Y. Xia, Y. S. Hor, D. Qian, A. V. Fedorov, H. Lin, A. Bansil, R. J. Cava, and M. Z. Hasan, Observation of topological order in a superconducting doped topological insulator, Nat. Phys. **6**, 855 (2010).

[3] M. I. Shalaev, W. Walasik, A. Tsukernik, Y. Xu, and N. M. Litchinitser, Robust topologically protected transport in photonic crystals at telecommunication wavelengths, Nat. Nanotechnol. **14**, 31 (2019).

[4] T. Ozawa, H. M. Price, A. Amo, N. Goldman, M. Hafezi, L. Lu, M. C. Rechtsman, D. Schuster, J. Simon, O. Zilberberg, and I. Carusotto, Topological photonics, Rev. Mod. Phys. **91**, 015006 (2019).

[5] P. St-Jean, V. Goblot, E. Galopin, A. Lemaître, T. Ozawa, L. L. Gratiet, I. Sagnes, J. Bloch, and A. Amo, Lasing in topological edge states of a one-dimensional lattice, Nat. Photonics **11**, 651 (2017).

[6] M. Parto, S. Wittek, H. Hodaei, G. Harari, M. A. Bandres, J. Ren, M. C. Rechtsman, M. Segev, D. N. Christodoulides, and M. Khajavikhan, Edge-mode lasing in 1D topological active arrays, Phys. Rev. Lett. **120**, 113901 (2018).

[7] J.-Q. Zhang, J.-X. Liu, H.-L. Zhang, Z.-R. Gong, S. Zhang, L.-L. Yan, S.-L. Su, H. Jing, and M. Feng, Topological optomechanical amplifier in synthetic PT-symmetry, Nanophotonics **11**, 1149 (2022).

[8] T. Ramos, J. J. García-Ripoll, and D. Porras, Topological input-output theory for directional amplification, Phys. Rev. A **103**, 033513 (2021).

[9] C. C. Wanjura, M. Brunelli, and A. Nunnenkamp, Topological framework for directional amplification in driven-dissipative cavity arrays, Nat. Commun. **11**, 3149 (2020).

[10] D. Porras and S. Fernández-Lorenzo, Topological amplification in photonic lattices, Phys. Rev. Lett. **122**, 143901 (2019).

[11] W. P. Su, J. R. Schrieffer, and A. J. Heeger, Solitons in polyacetylene, Phys. Rev. Lett. **42**, 1698 (1979).

[12] A. J. Heeger, S. Kivelson, J. R. Schrieffer, and W. P. Su, Solitons in conducting polymers, Rev. Mod. Phys. **60**, 781 (1988).

[13] A. Bansil, H. Lin, and T. Das, *Colloquium*: Topological band theory, Rev. Mod. Phys. **88**, 021004 (2016).

[14] X.-W. Xu, Y.-J. Zhao, H. Wang, A.-X. Chen, and Y.-X. Liu, Generalized Su-Schrieffer-Heeger model in one dimensional optomechanical arrays, Front. Phys. **9**, 813801 (2022).

[15] E. J. Meier, F. A. An, and B. Gadway, Observation of the topological soliton state in the Su-Schrieffer-Heeger model, Nat. Commun. **7**, 13986 (2016).

[16] T. Tian, Y. Zhang, L. Zhang, L. Wu, S. Lin, J. Zhou, C.-K. Duan, J.-H. Jiang, and J. Du, Experimental realization of nonreciprocal adiabatic transfer of phonons in a dynamically modulated nanomechanical topological insulator, Phys. Rev. Lett. **129**, 215901 (2022).

[17] N. E. Palaiodimopoulos, I. Brouzos, F. K. Diakonos, and G. Theocharis, Fast and robust quantum state transfer via a topological chain, Phys. Rev. A **103**, 052409 (2021).

[18] F. Mei, G. Chen, L. Tian, S.-L. Zhu, and S. Jia, Robust quantum state transfer via topological edge states in superconducting qubit chains, Phys. Rev. A **98**, 012331 (2018).

[19] C. Wang, L. Li, J. Gong, and Y.-X. Liu, Arbitrary entangled state transfer via a topological qubit chain, Phys. Rev. A **106**, 052411 (2022).

[20] L. Qi, G.-L. Wang, S. Liu, S. Zhang, and H.-F. Wang, Engineering the topological state transfer and topological beam splitter in an even-sized Su-Schrieffer-Heeger chain, Phys. Rev. A **102**, 022404 (2020).

[21] J. Cao, W.-X. Cui, X. X. Yi, and H.-F. Wang, Controllable photon-phonon conversion via the topologically protected edge channel in an optomechanical lattice, Phys. Rev. A **103**, 023504 (2021).

[22] L.-N. Zheng, X. Yi, and H.-F. Wang, Engineering a phase-robust topological router in a dimerized superconducting-circuit lattice with long-range hopping and chiral symmetry, Phys. Rev. Appl. **18**, 054037 (2022).

[23] L. Qi, N. Han, S. Liu, H.-F. Wang, and A.-L. He, Controllable excitation transmission and topological switch based on an imaginary topological channel in a non-Hermitian Su-Schrieffer-Heeger chain, Phys. Rev. A **107**, 062214 (2023).

[24] L. Qi, Y. Yan, Y. Xing, X.-D. Zhao, S. Liu, W.-X. Cui, X. Han, S. Zhang, and H.-F. Wang, Topological router induced via long-range hopping in a Su-Schrieffer-Heeger chain, Phys. Rev. Res. **3**, 023037 (2021).

[25] L. Qi, Y. Xing, X.-D. Zhao, S. Liu, S. Zhang, S. Hu, and H.-F. Wang, Topological beam splitter via defect-induced edge channel in the Rice-Mele model, Phys. Rev. B **103**, 085129 (2021).

[26] J. D. Brehm, A. N. Poddubny, A. Stehli, T. Wolz, H. Rotzinger, and A. V. Ustinov, Waveguide bandgap engineering with an array of superconducting qubits, npj Quantum Mater. **6**, 10 (2021).

[27] M. Zanner, T. Orell, C. M. F. Schneider, R. Albert, S. Oleschko, M. L. Juan, M. Silveri, and G. Kirchmair, Coherent control of a multi-qubit dark state in waveguide quantum electrodynamics, Nat. Phys. **18**, 538 (2022).

[28] A. Goban, C.-L. Hung, S.-P. Yu, J. D. Hood, J. A. Muniz, J. H. Lee, M. J. Martin, A. C. McClung, K. S. Choi, D. E. Chang, O. Painter, and H. J. Kimble, Atom-light interactions in photonic crystals, Nat. Commun. **5**, 3808 (2014).

[29] A. Goban, C.-L. Hung, J. D. Hood, S.-P. Yu, J. A. Muniz, O. Painter, and H. J. Kimble, Superradiance for atoms trapped along a photonic crystal waveguide, Phys. Rev. Lett. **115**, 063601 (2015).

[30] D. Roy, C. M. Wilson, and O. Firstenberg, *Colloquium*: Strongly interacting photons in one-dimensional continuum, Rev. Mod. Phys. **89**, 021001 (2017).

[31] I.-C. Hoi, A. F. Kockum, T. Palomaki, T. M. Stace, B. Fan, L. Tornberg, S. R. Sathyamoorthy, G. Johansson, P. Delsing, and C. M. Wilson, Giant cross–Kerr effect for propagating microwaves induced by an artificial atom, Phys. Rev. Lett. **111**, 053601 (2013).

[32] X. Zhang, E. Kim, D. K. Mark, S. Choi, and O. Painter, A superconducting quantum simulator based on a photonic-bandgap metamaterial, Science **379**, 278 (2023).

[33] A. Tiranov, V. Angelopoulou, C. J. van Diepen, B. Schrinski, O. A. D. Sandberg, Y. Wang, L. Midolo, S. Scholz, A. D. Wieck, A. Ludwig, A. S. Sørensen, and P. Lodahl, Collective super- and subradiant dynamics between distant optical quantum emitters, Science **379**, 389 (2023).

[34] A. F. van Loo, A. Fedorov, K. Lalumière, B. C. Sanders, A. Blais, and A. Wallraff, Photon-mediated interactions between distant artificial atoms, Science **342**, 1494 (2013).

[35] A. S. Sheremet, M. I. Petrov, I. V. Iorsh, A. V. Poshakinskiy, and A. N. Poddubny, Waveguide quantum electrodynamics: Collective radiance and photon-photon correlations, Rev. Mod. Phys. **95**, 015002 (2023).

[36] J. S. Douglas, H. Habibian, C.-L. Hung, A. V. Gorshkov, H. J. Kimble, and D. E. Chang, Quantum many-body models with cold atoms coupled to photonic crystals, Nat. Photonics **9**, 326 (2015).

[37] I. M. Georgescu, S. Ashhab, and F. Nori, Quantum simulation, Rev. Mod. Phys. **86**, 153 (2014).

[38] E. Kim, X. Zhang, V. S. Ferreira, J. Banker, J. K. Iverson, A. Sipahigil, M. Bello, A. González-Tudela, M. Mirhosseini, and O. Painter, Quantum electrodynamics in a topological waveguide, Phys. Rev. X **11**, 011015 (2021).

[39] D.-W. Wang, C.-S. Zhao, S.-L. Chao, R. Peng, J. Yang, Z. Yang, and L. Zhou, Simulating topological phases with atom arrays in an optical waveguide, Opt. Express **30**, 42347 (2022).

[40] Z. Wang, T. Jaako, P. Kirton, and P. Rabl, Supercorrelated radiance in nonlinear photonic waveguides, Phys. Rev. Lett. **124**, 213601 (2020).

[41] G. Calajó, F. Ciccarello, D. Chang, and P. Rabl, Atom-field dressed states in slow-light waveguide QED, Phys. Rev. A **93**, 033833 (2016).

[42] Y. Liu and A. A. Houck, Quantum electrodynamics near a photonic bandgap, Nat. Phys. **13**, 48 (2017).

[43] P. Y. Wen, K.-T. Lin, A. F. Kockum, B. Suri, H. Ian, J. C. Chen, S. Y. Mao, C. C. Chiu, P. Delsing, F. Nori, G.-D. Lin, and I.-C. Hoi, Large collective Lamb shift of two distant superconducting artificial atoms, Phys. Rev. Lett. **123**, 233602 (2019).

[44] S. John and J. Wang, Quantum electrodynamics near a photonic band gap: Photon bound states and dressed atoms, Phys. Rev. Lett. **64**, 2418 (1990).

[45] T. Shi, Y.-H. Wu, A. González-Tudela, and J. I. Cirac, Bound states in boson impurity models, Phys. Rev. X **6**, 021027 (2016).

[46] A. González-Tudela and D. Porras, Mesoscopic entanglement induced by spontaneous emission in solid-state quantum optics, Phys. Rev. Lett. **110**, 080502 (2013).

[47] A. Gonzalez-Tudela, D. Martin-Cano, E. Moreno, L. Martin-Moreno, C. Tejedor, and F. J. Garcia-Vidal, Entanglement of two qubits mediated by one-dimensional plasmonic waveguides, Phys. Rev. Lett. **106**, 020501 (2011).

[48] M. Bello, G. Platero, J. I. Cirac, and A. González-Tudela, Unconventional quantum optics in topological waveguide QED, Sci. Adv. **5**, eaaw0297 (2019).

[49] X.-L. Dong, P.-B. Li, T. Liu, and F. Nori, Unconventional quantum sound-matter interactions in spin-optomechanical-crystal hybrid systems, Phys. Rev. Lett. **126**, 203601 (2021).

[50] M. Ringel, M. Pletyukhov, and V. Gritsev, Topologically protected strongly correlated states of photons, New J. Phys. **16**, 113030 (2014).

[51] Y.-l. Ren, J.-k. Xie, X.-k. Li, S.-l. Ma, and F.-l. Li, Long-range generation of a magnon-magnon entangled state, Phys. Rev. B **105**, 094422 (2022).

[52] H. Zheng, D. J. Gauthier, and H. U. Baranger, Waveguide QED: Many-body bound-state effects in coherent and Fock-state scattering from a two-level system, Phys. Rev. A **82**, 063816 (2010).

[53] C. Vega, M. Bello, D. Porras, and A. González-Tudela, Qubit-photon bound states in topological waveguides with long-range hoppings, Phys. Rev. A **104**, 053522 (2021).

[54] X.-L. Dong, C.-P. Shen, S.-Y. Gao, H.-R. Li, H. Gao, F.-L. Li, and P.-B. Li, Chiral spin-phonon bound states and spin-spin interactions with phononic lattices, Phys. Rev. Res. **4**, 023077 (2022).

[55] P. Delplace, D. Ullmo, and G. Montambaux, Zak phase and the existence of edge states in graphene, Phys. Rev. B **84**, 195452 (2011).

[56] J. Zak, Berry's phase for energy bands in solids, Phys. Rev. Lett. **62**, 2747 (1989).

[57] C. I. Kvande, D. B. Hill, and D. Blume, Finite Su-Schrieffer-Heeger chains coupled to a two-level emitter: Hybridization of edge and emitter states, Phys. Rev. A **108**, 023703 (2023).

[58] N. V. Vitanov, A. A. Rangelov, B. W. Shore, and K. Bergmann, Stimulated Raman adiabatic passage in physics, chemistry, and beyond, Rev. Mod. Phys. **89**, 015006 (2017).

[59] H. Pu, P. Maenner, W. Zhang, and H. Y. Ling, Adiabatic condition for nonlinear systems, Phys. Rev. Lett. **98**, 050406 (2007).

[60] P. Krantz, M. Kjaergaard, F. Yan, T. P. Orlando, S. Gustavsson, and W. D. Oliver, A quantum engineer's guide to superconducting qubits, Appl. Phys. Rev. **6**, 021318 (2019).

[61] A. Blais, A. L. Grimsmo, S. M. Girvin, and A. Wallraff, Circuit quantum electrodynamics, Rev. Mod. Phys. **93**, 025005 (2021).

[62] D. Vion, A. Aassime, A. Cottet, P. Joyez, H. Pothier, C. Urbina, D. Esteve, and M. H. Devoret, Manipulating the quantum state of an electrical circuit, Science **296**, 886 (2002).

[63] I. Buluta and F. Nori, Quantum simulators, Science **326**, 108 (2009).

[64] M. Fitzpatrick, N. M. Sundaresan, A. C. Y. Li, J. Koch, and A. A. Houck, Observation of a dissipative phase transition in a one-dimensional circuit QED lattice, Phys. Rev. X **7**, 011016 (2017).

[65] C. Noh and D. G. Angelakis, Quantum simulations and many-body physics with light, Rep. Prog. Phys. **80**, 016401 (2017).

[66] A. J. Daley, I. Bloch, C. Kokail, S. Flannigan, N. Pearson, M. Troyer, and P. Zoller, Practical quantum advantage in quantum simulation, Nature (London) **607**, 667 (2022).

[67] A. Blais, J. Gambetta, A. Wallraff, D. I. Schuster, S. M. Girvin, M. H. Devoret, and R. J. Schoelkopf, Quantum-information processing with circuit quantum electrodynamics, Phys. Rev. A **75**, 032329 (2007).

[68] M. Mirhosseini, E. Kim, X. Zhang, A. Sipahigil, P. B. Dieterle, A. J. Keller, A. Asenjo-Garcia, D. E. Chang, and O. Painter, Cavity quantum electrodynamics with atom-like mirrors, Nature (London) **569**, 692 (2019).

[69] L. Leonforte, A. Carollo, and F. Ciccarello, Vacancy-like dressed states in topological waveguide QED, Phys. Rev. Lett. **126**, 063601 (2021).

[70] A. A. Houck, H. E. Türeci, and J. Koch, On-chip quantum simulation with superconducting circuits, Nat. Phys. **8**, 292 (2012).

[71] S. Schmidt and J. Koch, Circuit QED lattices: Towards quantum simulation with superconducting circuits, Ann. Phys. (NY) **525**, 395 (2013).

[72] A. Somoroff, Q. Ficheux, R. A. Mencia, H. Xiong, R. Kuzmin, and V. E. Manucharyan, Millisecond coherence in a superconducting qubit, Phys. Rev. Lett. **130**, 267001 (2023).

[73] K. Bergmann, H. Theuer, and B. W. Shore, Coherent population transfer among quantum states of atoms and molecules, Rev. Mod. Phys. **70**, 1003 (1998).